J Comp Physiol A (2010) 196:659–668
DOI 10.1007/s00359-010-0556-y

ORIGINAL PAPER

Material properties of the skin of the Kenyan sand boa *Gongylophis colubrinus* (Squamata, Boidae)

Marie-Christin G. Klein · Julia K. Deuschle · Stanislav N. Gorb

Received: 11 May 2010 / Revised: 21 June 2010 / Accepted: 22 June 2010 / Published online: 10 July 2010

Abstract On the basis of structural data, it has been previously assumed that the integument of snakes consists of a hard, robust, inflexible outer surface (*Oberhäutchen* and *β*-layer) and soft, flexible inner layers (*α*-layers). The aim of this study was to compare material properties of the outer and inner scale layers of the exuvium of *Gongylophis colubrinus*, to relate the structure of the snake integument to its mechanical properties. The nanoindentation experiments have demonstrated that the outer scale layers are harder, and have a higher effective elastic modulus than the inner scale layers. The results obtained provide strong evidence about the presence of a gradient in the material properties of the snake integument. The possible functional significance of this gradient is discussed here as a feature minimizing damage to the integument during sliding locomotion on an abrasive surface, such as sand.

Keywords Effective elastic modulus · Nanoindentation · Gradient materials · Biological materials · Wear resistance

M.-C. G. Klein (✉) · S. N. Gorb
Department of Functional Morphology and Biomechanics, Zoological Institute of the University of Kiel, Am Botanischen Garten 1-9, 24098 Kiel, Germany
e-mail: mklein@zoologie.uni-kiel.de

S. N. Gorb
e-mail: sgorb@zoologie.uni-kiel.de

M.-C. G. Klein · J. K. Deuschle · S. N. Gorb
Evolutionary Biomaterials Group, Max Planck Institute for Metals Research, Heisenbergstr. 3, 70569 Stuttgart, Germany
e-mail: deuschle@mf.mpg.de

Introduction

Snakes are limbless reptiles that use their entire body for sliding locomotion. This supposes that the epidermis, at least that of the ventral body side, has to permanently endure friction forces. One can expect some specializations in the snake epidermis, against abrasion. Even though snakes from different lineages have different body size, scale dimension, body shape and body mass (Mattison 1995) their epidermis basically consists of six layers overlying the dermis (Baden and Maderson 1970; Landmann 1979) (Fig. 1c). The following epidermis layers from the outer scale surface towards the dermis are known (Fig. 1c): (1) the *Oberhäutchen*, (2) *β*-layer, (3) mesos-layer, (4) *α*-layer, (5) lacunar tissue and (6) clear layer.

During maturation of the epidermis, the relatively thin *Oberhäutchen* fuses together with the thick *β*-layer resulting in a homogeneous *stratum* without cell boundaries. In the lowermost region of the *β*-layer, cell boundaries are still recognizable (Landmann 1979). When combined together these two layers compose the outer surface of the snake epidermis, which interacts with the environment. The next layers, underlying this relatively thick outer shell, are so-called *α*-layers composed of *α*-keratin (Gregg and Rogers 1986; Sawyer et al. 2000; Alibardi and Sawyer 2002). The mesos-layer consists of 2–10 layers of flattened cells containing *α*–filaments, which do not form a matrix keratin pattern. The *α*-layer consists of several keratinized cell layers (number of layers can vary according to species and seasonal influence, perhaps even in one species) and contains *α*-keratin (mammalian-type) with a coiled-coil conformation rather than *β*-keratin (bird-type) with a pleated sheet conformation present in the *β*-layer (Landmann 1979, 1986; Irish et al. 1988). The lacunar tissue and the clear layer make up the inner most part of the epidermis. The clear layer

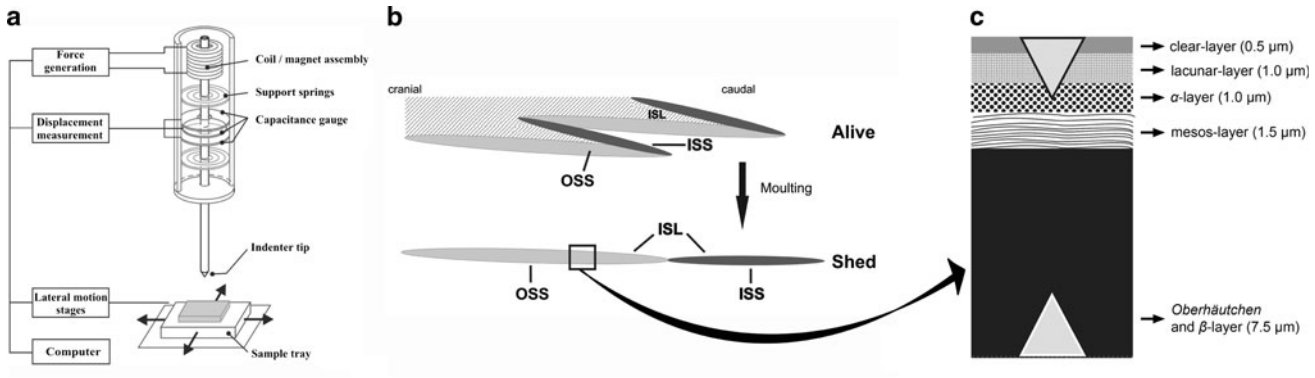

Fig. 1 Schematic drawing of the indentation system setup with the coil-magnet assembly for load application, the capacitive displacement sensor and the indenter shaft support springs (Barbakadze et al. 2006) (**a**). Schematic drawing of a shedding cycle on scale level. The *black square* illustrates the skin part which was tested (**b**). Diagram of the cross section of the snake integument (after Landmann 1986; Maderson et al. 1998, Toni and Alibardi 2007 and the present study). *Triangles* indicate the indentation depth undertaken in this study (**c**). *ISL* inner scale layers, *ISS* inner scale surface, *OSS* outer scale surface

lies directly above the *stratum germativum*. The lacunar tissue consists of 1–4 cell layers. The clear layer consists of one layer of flattened cells. Both layers are similar and their cells resemble immature α-cells (Landmann 1979, 1986).

Snakes shed their entire skin (Irish et al. 1988) 4–8 times a year depending on the species. Moulting provides the renewal of the epidermis, but is not likely to be the only adaptation against wear because frequent moulting is costly from an energetic point of view. In addition, scratches in the outermost layer of the skin may affect frictional properties of the skin and lead to further increase in abrasion. Both the exuvium surface geometry is not different from that of an intact animal, since the new epidermis is developed as a copy of an underneath old epidermis. In a living snake, each scale has two sides exposed to the environment [both of them are here called the outer scale layer (OSL)] (1) the outer scale surface (OSS) is in contact with the substrate and (2) the inner scale surface (ISS) is in contact to the following scale. Both the outer and inner scale surfaces are composed of the six above-mentioned cell layers. The epidermis side facing the *stratum germativum* is here called the inner scale layer (ISL). The ISLs become unfolded and exposed after the skin has been shed (Fig. 1b).

Previous authors have hypothesized that the presumably softer α-keratin (Maderson 1964; Alexander 1970; Baden and Maderson 1970; Matoltsy 1976; Wyld and Brush 1979; Furch and Marchuk 1983; Landmann 1986; Carver and Sawyer 1987; O'Guin et al. 1987; Alibardi and Toni 2006a, b, c) is responsible for the flexibility of the α-layer, whereas β-keratin makes the β-layer inflexible (Mercer 1961; Maderson 1964; Matoltsy 1976; Landmann 1986). The β-layer was hypothesized to be a strengthening layer against mechanical and chemical injuries (Landmann 1979). This hypothesis is based, among others, on the data of Baden and Maderson (1970), who showed that matrix proteins of β-keratin contain 7.4% half cystine linked by disulfide bonds, whereas the matrix proteins of α-keratin only contain 6.5%. In addition, the *Oberhäutchen* contains a large amount of matrix material (Landmann 1979). Furthermore, the number of stable disulfide bonds tends to increase from the inside outward through the keratinized layers of the epidermis (Goslar 1958; Banerjee and Mittal 1978). The cell boundaries in squamata *Oberhäutchen* and β-layers are dissolved completely, in contrast to β-keratin in feathers (Filshie and Rogers 1962). Additionally, both the mesos- and clear layer contain a keratin network (Landmann 1979), which in combination with a reduced matrix is suggested to be rather flexible (Matoltsy 1976). In the α-layers, the marginal layer of α-keratin containing cells decreases in thickness from without inwards (Landmann 1979), which could be associated with a gradient. The dermis, which lies beneath the epidermis, consists among other components, such as capillaries of various fibers, and is less stiff as compared to the epidermis (Landmann 1979).

The aim of this study was to compare local material properties of the outer and inner scale layers of the exuvium to test previous hypotheses about the contribution of the structure and composition of the snake integument to its material properties. The exuvium of the Kenyan sand boa *Gongylophis colubrinus* (Squamata, Boidae) (Fig. 2a) was used in the experiment. *G. colubrinus* inhabits the desert and moves through the sand or on it. Thus, its ventral epidermis is under pressure, and is continuously in contact with highly abrasive sand particles. This snake, occupying a habitat similar to the sand skink (*Scincus scincus*), has been previously suggested to have a very robust epidermis, which exhibits low friction and high abrasion resistance (Rechenberg and El Khyari 2004).

Using the nanoindentation technique, both the effective elastic modulus and hardness of the outer and inner epidermis layers were characterized and compared. This method, allowing characterization of material properties at

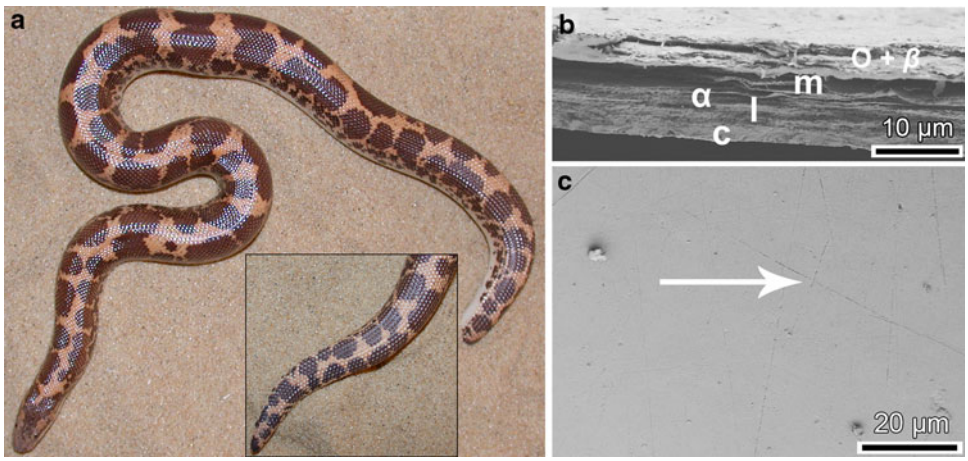

Fig. 2 Body (**a**), tail region (**a** *inset*) and SEM images of the ventral scales of *G. colubrinus*. Fracture of a ventral scale of an exuvium showing different epidermis layers (outer scale surface is on the *top* of the *image*) (**b**). Caudal part of a ventral scale of an exuvium illustrating abrasion marks on the *Oberhäutchen* (*arrow*) (**c**). *O* + *β Oberhäutchen* + *β*-layer, *m* mesos-layer, *α* *α*-layer, *l* lacunar tissue, *c* clear layer

the local level, has been previously used to evaluate mechanical properties on small volumes of various biological materials (Arzt et al. 2002; Enders et al. 2004; Barbakadze et al. 2006). The results obtained in the present study provide strong evidence about the presence of a gradient in material properties of the snake integument.

Materials and methods

The nanoindentation measurements were conducted using exuvia from an adult *G. colubrinus* male (Fig. 2a). Cryo scanning electron microscopy was conducted using snake samples, obtained from the University of Bonn. The samples were kept in a −20°C deep freezer subsequently after death.

Nanoindentation

Nanoindentation is a technique to measure mechanical properties of thin and heterogeneous samples with small volumes (Oliver and Pharr 1992; Xu et al. 1998; Ebenstein and Pruitt 2006). Through the force–displacement curves obtained using this technique, hardness and modulus of the material can be determined (Oliver and Pharr 1992) for penetration depths as small as several hundred nanometers (Enders et al. 2004). The equations used to extract hardness and elasticity information from force–displacement curves according to Oliver and Pharr (1992; 2004) are as follows:

$$H = \frac{p_{\max}}{A_c}, \quad (1)$$

where H is hardness, $P_{\max}$ is the maximal load and A_c is the contact area,

$$E_{\text{eff}} = \frac{\sqrt{\pi}}{2}\frac{S}{\beta\sqrt{A_c}} \quad (2)$$

with E_{eff} being the reduced or effective elastic E modulus, β the correction factor for the indenter form, and S the contact stiffness. In contrast to the Young's modulus, the effective elastic modulus can be determined by means of nanoindentation. Furthermore, since the Poisson coefficient is not known the elastic modulus could not be determined. Due to the variation of material structure depending on the depth in biological samples, the mechanical properties might fluctuate considerably with depth (Enders et al. 2004). Therefore, the continuous stiffness measurement method was applied, which allows a continuous measurement of mechanical properties as a function of depth (Oliver and Pharr 1992; Enders et al. 2004). Although the Oliver–Pharr method is mainly meant for isotropic materials and therefore is not ideal for anisotropic biological material, it is the best method to date for studies of material properties. In our previous work, we successfully applied this method for mechanical characterization of biological samples (Arzt et al. 2002; Enders et al. 2004; Barbakadze et al. 2006). Furthermore, this method is valid for our anisotropic material because we are comparing both sides of a biological material in relation to one another using relative and not absolute values and the comparability with previous results from former studies is given.

The Nano Indenter SA2 (MTS Nano Instruments, Oak Ridge, TN, USA) (Fig. 1a) was used in this study. This system allows testing of materials with low contact stiffness, such as soft biological tissues or gels (Enders et al. 2004; Deuschle et al. 2007). A standard Berkovich indenter tip was used in all experiments. This tip is a three-sided pyramid with a face opening angle of 65.3° (Enders et al. 2004). The tests were conducted under normal room conditions (relative humidity 40–45%, temperature 22–25°C). During each test, the relative humidity was kept constant and the temperature fluctuations were recorded to be below ±0.5°C.

Sample preparation for nanoindentation

Exuvia pieces (5 × 5 mm) of *G. colubrinus* were cut from the ventral scales of the mid-body region and attached to an

aluminum sample holder with 5925 cyanacrylat superglue (Kisling AG, Schwäbisch Hall, Germany). The samples were fixed in one of two ways: (1) the outer scale layers, the *Oberhäutchen*/*β*-layer, of the outer scale surface were facing the indenter tip; (2) the inner scale layers, clear layer, of the outer scale surface was facing the tip (Fig. 1b). This way the mechanical properties into the direction perpendicular to the surface and therefore out-of-plane regarding the keratin fibers were obtained. The results acquired from this experimental setup, in contrast to in-plane indentation, are relevant for our study since the forces exerted on the snake skin are mainly out-of-plane. For each surface, three different individual scales were prepared. 12–19 indentation tests, on the posterior edge of the scale, were carried out on each individual scale.

Nanoindentation test procedure

All tests on one sample were performed within 1 h to minimize noise in the data, caused by changes in the environmental conditions of the laboratory. The samples were loaded under constant strain rate conditions, with a rate of 0.05 s^{-1} to a maximum penetration depth of 2 µm. Before the sample was fully unloaded the maximum load was reduced to 95% and the thermal drift was measured. Thereafter, the indenter tip was moved to the next preselected test location. To ensure proper surface detection, the procedure described in Deuschle et al. (2007) was used. After the tests were completed, each indentation curve was manually processed to verify a correct surface approach.

Preparation for scanning electron microscopy of the cross sections

5 × 10 mm pieces of exuvia and scale margins of fresh skin (kept frozen at −20°C) were cut from the ventral scale region and mechanically fixed on a specimen holder in a vertical position relative to the holder plane, so that the fractured integument could be examined in the cross section. The mounted samples were blown with a jet of compressed air to remove dust particles, frozen in liquid nitrogen and then fractured using a cold metal knife at −140°C in the Gatan ALTO 2500 Cryo preparation system. After coating with gold palladium (6 nm thickness and a rate of 1:9), the samples were observed in a Hitachi-S4800 (Tokyo, Japan) scanning electron microscope at the temperature of −120°C and accelerating voltage of 2–3 kV. Exuvia were also examined using the Hitachi-S4800 (Tokyo, Japan) SEM, although at room temperature.

Preparation for scanning electron microscopy of the scale structures

5 × 10 mm pieces of ventral, dorsal and lateral scale regions of a *G. colubrinus* exuvia were cut and mechanically fixed on a specimen holder, so that the outer scale surface of the integument could be examined. The mounted samples were then prepared as described above and observed in the SEM at an accelerating voltage of 2–3 kV.

Results

The epidermis of *G. colubrinus* shows a variation in scale microstructure, when comparing the ventral and lateral sides with the dorsal side of the body (Fig. 3). Dorsal, ventral and lateral scales have in common that the outer scale surface bears strap-shaped *Oberhäutchen* cells, which exhibit pits. The cells have caudal elevations and random denticulations from the cranial to the central part of the scale (Fig. 3a). However, in contrast to the dorsal scales, which bear denticulations aligned in comb-like rows running perpendicular to the longitudinal body axis on the caudal scale part and have a central ridge, the lateral and ventral scales are relatively smooth from the central to the caudal part of the scale (Fig. 3b).

The ventral epidermis of a *G. colubrinus* exuvium is about 12 µm thick. The layered organization of the epidermis layers is clearly visible in fractures of both exuvia and fresh scales (Figs. 2b, 4a, b). Abrasion marks were often seen on the outer scale surface (*Oberhäutchen*) of a ventral exuvium scale (Fig. 2c).

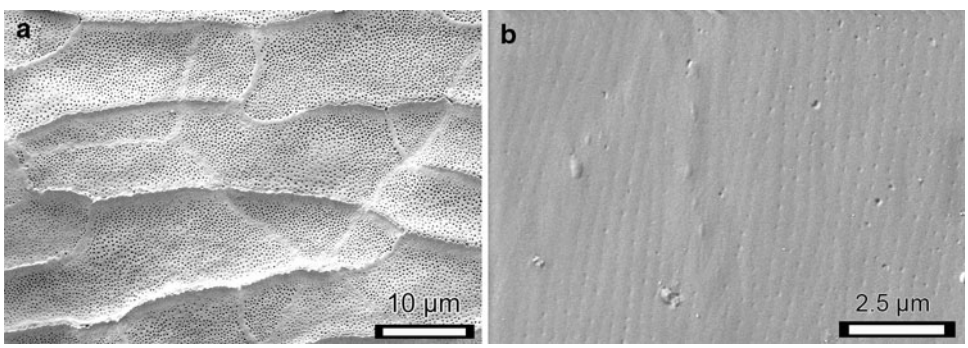

Fig. 3 *G. colubrinus*, SEM images illustrating the microstructure of the Oberhäutchen on the outer ventral scale surface. Cranial (**a**) and caudal (where the indentation experiments were conducted) (**b**) part of a ventral scale. *Image bottom* indicates caudal direction

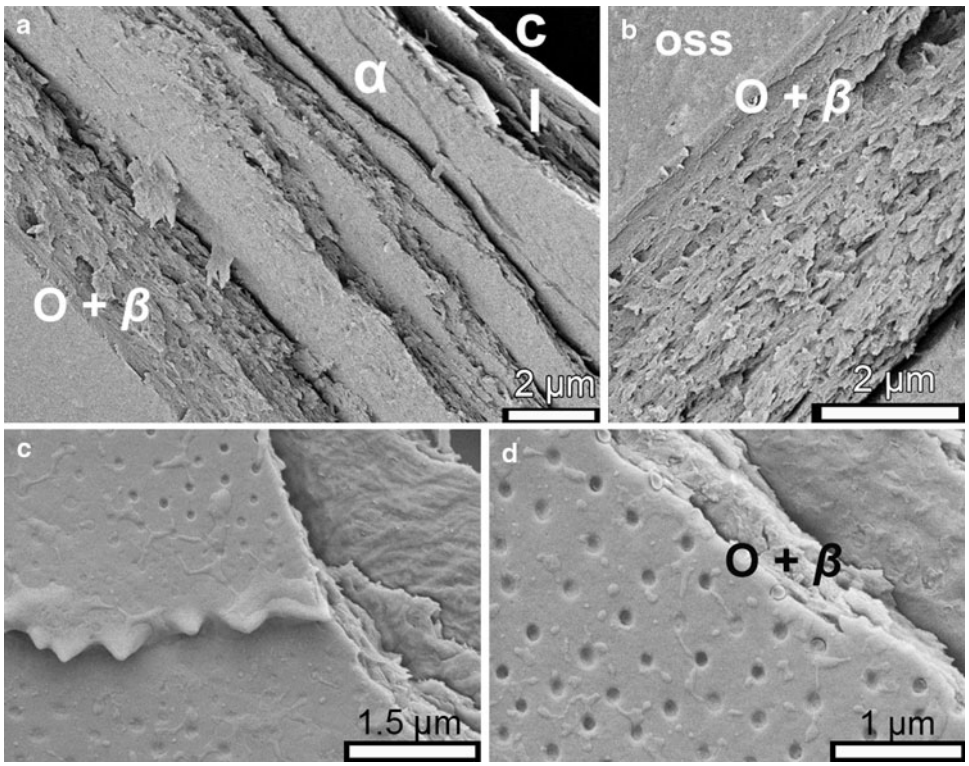

Fig. 4 *G. colubrinus*, Cryo-SEM of ventral scales. Profile of a fresh scale with an overview (**a**) of the epidermis layers and a detailed view (**b**) of the *β*-layer. The outer scale surface (*OSS*) is in the bottom *left* (**a**) or *top left* (**b**). Rostral *OSS* part of a fresh scale shown from above (**c**). Caudal *OSS* part of a fresh scale shown from above (**d**). *O* + *β* *Oberhäutchen* + *β*-layer, *m* mesos-layer, *α* *α*-layer, *l* lacunar tissue, *c* clear layer, *OSS* outer scale surface

Taking into consideration the indentation depth, applied in this study (Fig. 1c), the information about mechanical response was collected from the outer regions of the *Oberhäutchen* + *β*-layer (outer surface) and from the *α*-layers (inner surface). The hardness and effective elastic modulus values for the exuvia samples were studied as a function of the indentation depth (Fig. 5). No significant difference was found, when comparing the measurement series separately for either the inner or outer scale surface for each scale tested. The load–displacement curves revealed a significant difference in the mechanical response, and thus in the modulus values obtained for the outer (4.1 GPa) and inner (3.2 GPa) scale layers (Table 1; $p < 0.001$, one-way RM ANOVA and *t* test). There was also a statistically significant difference between hardness values of the outer (0.28 GPa) and inner (0.14 GPa) scale layers (Table 1; $p < 0.001$, one-way RM ANOVA and *t* test).

Figure 5b, c shows that the modulus and hardness values change with indentation depth for both the inner and the outer scale layers. Table 2 shows the modulus and hardness values for the inner and outer scale layers within three intervals (400–500, 1,000–1,100 and 1,600–1,700 nm). When comparing data obtained within these depth intervals, the modulus values increase with indentation depth for the successive inner scale layers (3.30, 3.43 and 3.48 GPa) and decrease for the successive outer scale layers (5.02, 4.73 and 4.46 GPa), whereas the hardness values do not change significantly (Table 2).

Tables 3 and 4 present differences between modulus and hardness results measured at various depths for the indentation from inner (Table 3) and outer (Table 4) directions. The comparison within the inner scale layers shows that the only significant difference for the modulus was found between ranges of depth of 400–500 and 1,600–1,700 nm. This would suggest a fine transition of the modulus from the inside to the outside. When looking at the hardness values for the inner scale layers, only hardness measured in the depth ranges 400–500 and 1,600–1,700 nm shows no significant difference. This would suggest that inner layers start out hard, become less hard at a depth of 1,000 nm and then become harder again, when the indenter reaches the *α*-layer.

When comparing modulus values for outer scale layers, all three depth intervals show significant differences between each other. In hardness, there is only a significant difference between depth intervals 400–500 and 1,000–1,100 nm.

Discussion

Our results of the nanoindentation tests on ventral *G. colubrinus* scales provide strong evidence for the existence of a gradient in material properties across the ventral epidermis of the sand boa. Because the snake epidermis consists of dead cells or cellular derivatives (Irish et al. 1988), we assume no discrepancy in material properties

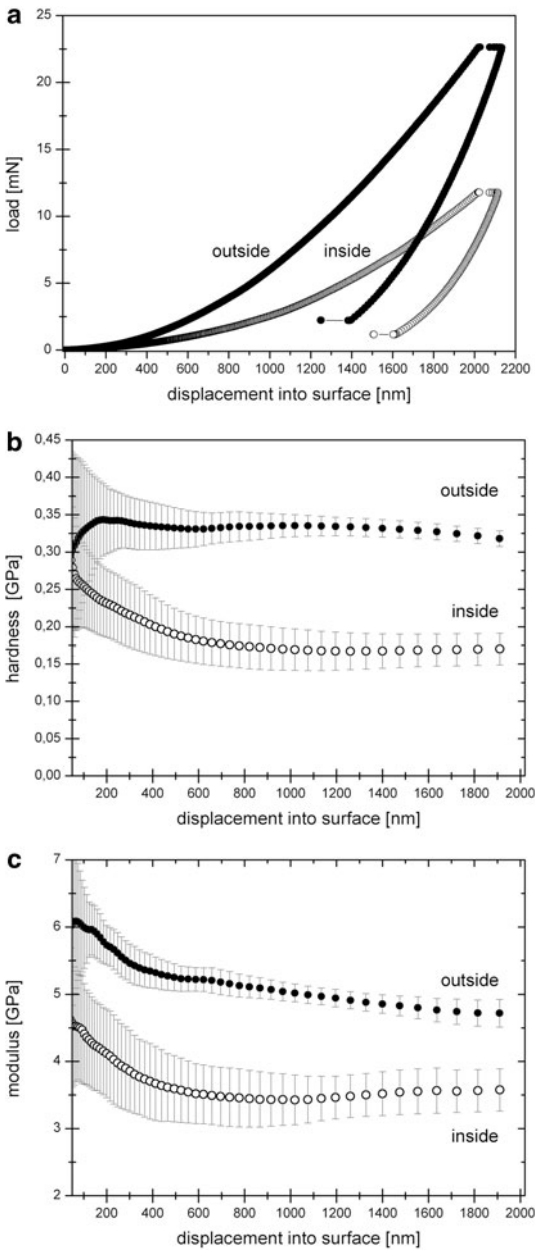

Fig. 5 Results of nanoindentation measurements for both the outer and inner scale layers. Load–displacement curves (**a**). Hardness versus displacement (**b**). Effective elastic modulus versus displacement (**c**). *Each curve* represents the average of at least 12 tests and the *error bars* denote standard deviations

between fresh and shed epidermis. The outer scale layers are harder and exhibit a higher effective elastic modulus than the inner scale layers containing only a reduced keratin matrix. The data correlates well with antibody labeling results showing the distribution of α- and β-keratin within molts of juveniles of the python *Lasius fuscus* and the colubrid snake *Natrix natrix* (Toni and Alibardi 2007), whereas the hard β-keratin is only present in the β-layer. In addition, variations in the measured moduli at different depths may also be explained by recent studies (Dalla Valle et al. 2005; Alibardi and Toni 2006a, b, c; Toni and Alibardi 2007), which have shown that there are at least three different types of β-keratins. For instance some that corresponds to glycine–proline-rich proteins that associate to α-keratin bundles and are responsible for the hardening of the reptilian epidermis. These proteins are temporarily synthesized at high levels in the *Oberhäutchen* and β-layer. Synthesis decreases and stops in layers underlying these (mesos- and α-layers) (Landmann 1986). Moreover, Toni and Alibardi (2007) differentiate, among others, between β-keratins that appear as basic proteins and β-keratins associated with cytokeratins as matrix proteins. However, our nanoindentation method did not have enough in-depth resolution to mechanically characterize such fine sub-layers.

The mean values of the modulus and hardness obtained for the outer (4.9 and 0.27 GPa) and inner scale layers (3.1 and 0.13 GPa) are comparable with the results, obtained in other studies on the mechanical properties of keratinous materials (Bonser and Purslow 1995; Moran et al. 2007; Huber et al. 2008). The hardness and modulus values for the inner scale layers are relatively high close to the surface (Fig. 5b, c). This can be explained by the fact that the tip oscillation (independent of the amplitude) affects the contact formation as well as contact stabilization for displacements between 0 and approximately 300 nm and thus results obtained at these shallow depths are not reliable to make any conclusion (Deuschle 2008).

Modulus values for β-keratin range between 1.0 and 8.0 GPa (Bonser and Purslow 1995; Bonser 2001; Huber et al. 2008) and the values for α-keratin are also quite variable (modulus 3.0–7.5 GPa; hardness 0.1–0.4 GPa) (Farren et al. 2004; Wei et al. 2005; Moran et al. 2007). This means material properties of biological materials preferably containing either β- or α-keratin vary more than would be expected. One can assume that it is not only the keratin type which influences hardness and elasticity, but also the arrangement of filaments (Fraser and MacRae 1980) and the architecture of the keratin matrix, for instance the thickness of the β- and α-keratin layers. The material ultrastructure of the snake's integument (relatively tight packaging of layers) or the bird feather (hollow feather shaft) influences material properties according to the specific function of the material. For instance, Bonser (2001) found that the rachis of two different feather types of the Ostrich revealed two significantly different moduli. The keratin composite of the wing feather had a modulus of 1.71 GPa and the body contour feather of 2.42 GPa. Bonser (2001) argues that the difference in moduli might tell us something about the mechanical loads to which the feathers are subjected. The mechanical environment of contour feathers might be more demanding than that of flight feathers. It was also suggested that strain in feathers will depend on both rachis shape and

Table 1 Mean and standard deviation values of hardness and effective elastic modulus measurements on the inner scale layers (ISL) and outer scale layers (OSL) of three different ventral scales of *G. colubrinus* exuvium

ISL			OSL			
Measurement	Mean (GPa)	SD (GPa)	Measurement	Mean (GPa)	SD (GPa)	
Effective elastic modulus						
1 ($n = 19$)	3.15	0.31	1 ($n = 16$)	4.86	0.13	$p < 0.01$, t test
2 ($n = 12$)	3.30	0.28	2 ($n = 20$)	4.98	0.15	$p < 0.01$, Tukey's test
3 ($n = 14$)	3.55	0.35	3 ($n = 16$)	4.91	0.25	$p < 0.01$, t test
Pooled ($n = 45$)	3.16	0.30	Pooled ($n = 52$)	4.13	0.34	$p < 0.01$, Tukey's test
Hardness						
1 ($n = 19$)	0.13	0.02	1 ($n = 16$)	0.27	0.03	$p < 0.01$, t test
2 ($n = 12$)	0.16	0.02	2 ($n = 20$)	0.35	0.02	$p < 0.01$, t test
3 ($n = 14$)	0.18	0.03	3 ($n = 16$)	0.34	0.01	$p < 0.01$, Tukey's test
Pooled ($n = 45$)	0.14	0.02	Pooled ($n = 52$)	0.28	0.02	$p < 0.01$, Tukey's test

Statistical comparison was carried out using the t test and one-way RM ANOVA

Table 2 Comparison of the mean and standard deviation values of hardness and effective elastic modulus measured at three different indentation depth intervals (400–500, 1,000–1,100 and 1,600–1,700 nm) of the inner scale layers (ISL) and outer scale layers (OSL) of all three *G. colubrinus* scales tested

ISL			OSL			
Depth range (nm) ($n = 45$)	Mean (GPa)	SD (GPa)	Depth range (nm) ($n = 52$)	Mean (GPa)	SD (GPa)	
Effective elastic modulus						
400–500	3.30	0.36	400–500	5.02	0.59	$p < 0.01$, Tukey's test
1,000–1,100	3.43	0.56	1,000–1,100	4.73	0.23	$p < 0.01$, Tukey's test
1,600–1,700	3.48	0.36	1,600–1,700	4.46	0.18	$p < 0.01$, Tukey's test
Hardness						
400–500	0.15	0.03	400–500	0.31	0.07	$p < 0.01$, Tukey's test
1,000–1,100	0.17	0.05	1,000–1,100	0.32	0.04	$p < 0.01$, Tukey's test
1,600–1,700	0.15	0.03	1,600–1,700	0.32	0.03	$p < 0.01$, Tukey's test

Statistical comparisons were carried out using one-way RM ANOVA

Table 3 Comparison of the mean and standard deviation values measured at three different depth intervals (400–500, 1,000–1,100 and 1,600–1,700 nm) of hardness and effective elastic modulus on the inner (ISL) scale layers of all three *G. colubrinus* scale tested

Depth range (nm) ($n = 45$)	Mean (GPa)	SD (GPa)	Depth range (nm) ($n = 45$)	Mean (GPa)	SD (GPa)	
Effective elastic modulus						
400–500	3.30	0.36	1,000–1100	3.43	0.56	NS
1,000–1,100	3.43	0.56	1,600–1,700	3.48	0.36	NS
1,600–1,700	3.48	0.36	400–500	3.30	0.36	$p = 0.01$, Tukey's test
Hardness						
400–500	0.15	0.03	1,000–1,100	0.17	0.05	$p < 0.01$, Tukey's test
1,000–1,100	0.17	0.05	1,600–1,700	0.15	0.03	$p < 0.01$, Tukey's test
1,600–1,700	0.15	0.03	400–500	0.15	0.03	NS

Statistical comparisons were carried out using one-way RM ANOVA

keratin properties (Bonser 2001). Thus, the feather geometry and the material ultrastructure are important features in determining the mechanical behavior of a whole feather (Astbury and Bell 1939). Furthermore, the method used in order to gain information on material properties (tensile, bending and nanoindentation tests) may also play a role in

Table 4 Comparison of the mean and standard deviation values measured at three different depth intervals (400–500, 1,000–1,100 and 1,600–1,700 nm) of hardness and effective elastic modulus on the outer scale layers (OSL) of all three *G. colubrinus* scale tested

Depth range (nm) ($n = 52$)	Mean (GPa)	SD (GPa)	Depth range (nm) ($n = 52$)	Mean (GPa)	SD (GPa)	
Effective elastic modulus						
400–500	5.02	0.59	1,000–1,100	4.73	0.23	$p < 0.01$, Tukey's test
1,000–1,100	4.73	0.23	1,600–1,700	4.46	0.18	$p < 0.01$, Tukey's test
1,600–1,700	4.46	0.18	400–500	5.02	0.59	$p < 0.01$, Tukey's test
Hardness						
400–500	0.31	0.07	1,000–1,100	0.32	0.04	$p = 0.05$, Tukey's test
1,000–1,100	0.32	0.04	1,600–1,700	0.32	0.03	NS
1,600–1,700	0.32	0.03	400–500	0.31	0.07	NS

Statistical comparisons were carried out using one-way RM ANOVA

varying values (Huber et al. 2008). This would explain the variation of values for β-keratin and for α-keratin and between the two.

Experiments carried out by Licht and Bennett (1972) on scaleless snakes showed that the β-layer contrary to previous data does not function as a permeability barrier. On the basis of these results and his own ones, Landmann (1979) suggested that the β-layers' main function is to protect the epidermis against abrasion. Toni and Alibardi (2007) showed that the α- and β-keratin differ in chemical structure and therefore presumably also in material properties (Matoltsy 1976). The β-keratin molecule is stiff and inelastic, which presumably makes materials containing it, more robust and therefore protecting the underlying layers against damage, whereas the α-keratin presumably provides flexibility to the material of the skin (Matoltsy 1976; Landmann 1979).

The epidermis of both the sand boa *G. colubrinus* and the sand skink *S. scincus* possess high durability and friction reducing properties (Rechenberg and El Khyari 2004). These authors suggested that these specific properties of the skink skin, and perhaps sand swimming reptiles in general are due to the microstructure on the scale surface. They supposed that microstructures reduce the effective contact area to the sand particles and may serve as sites for electrostatic charge concentration. The charges may enhance the repulsive force between skin and substrate that may lead to the wear reduction. Baumgartner et al. (2007) suggested that the low friction and high abrasion resistance of the sand skink skin is due to specific material properties that rely on the glycosylation of keratins.

Data of our study show for the first time hardness and effective elastic modulus values at different depths of the snake skin. This gives rise to an additional hypothesis that may explain high abrasion resistance due to a gradient in material properties of the integument from a hard and inflexible outside to a soft and elastic inside. There are other biological materials, such as cartilage, tooth, bone and wood which have to cope with abrasion and friction. Some of these systems have a similar layered structure with gradient material properties. It has previously been shown that in the tooth, such layered organization with the gradient of material properties is a key mechanism of the wear resistance (Wang and Weiner 1998; Fong et al. 2000). The visible part of the tooth, above the gum, is enveloped by the enamel, which is mechanically hard (Zheng et al. 2003) and highly resistant to wear (Fong et al. 2000). Its primary function is to protect the underlying dentin (the tooth's major component) and the more flexible and soft pulp (Zheng et al. 2003). Nanoindentation tests have shown that enamel is five times harder than dentin and possesses a three times higher elastic modulus (Fong et al. 2000). Using indentation tests on pulp and pulpless dog teeth with the Knoop indentor, Fusayama and Maeda (1968) showed that the dentin hardness in pulpless teeth is lower than that of vital teeth. The authors believe this to be due to the absence of the pulp functioning as a damping layer for the stiffer dentin.

A system which has to endure high amounts of stress under pressure is more effective against abrasion wear, if it has a gradient in structure and properties, since such design leads to more uniform stress distribution and thus to the minimization of the probability of local stress concentration (Gibson and Ashby 1988; Wang and Weiner 1998), which leads to the materials fatigue and failure. Since a hard, inflexible system will break easily under pressure and a flexible system will be easily worn off, the gradient material will improve wear resistance by combining advantages of both stiffness (outside) and flexibility (inside).

The β-layer of the snake skin can also be compared by analogy with some technical surface developments, such as diamond-like carbon (DLC) coatings. Nanoindentation tests showed that DLC layers have much higher hardness values (14–18 GPa) than those of coated materials (Xu and Rowcliffe 2002). That is why DLC coatings have low friction coefficients (Lettington 1998), which in combination with more compliant underlying materials make them useful for protecting objects from scratches.

Conclusion and outlook

The microscopy data provide evidence for the presence of a structural gradient in the ventral epidermis. The nanoindentation results demonstrate the presence of the gradient in the material properties of the snake skin. Taken together, these two facts may suggest that the structural gradient is responsible for a gradient of mechanical properties, which might represent one of the mechanisms reducing abrasion of the snake skin. Further comparative data on different body regions of different snakes, as well as the local experimental testing of the skin wear, might aid in the understanding of the role of structural and mechanical features of the skin in abrasion reduction.

Acknowledgments Dr. Guido Westhoff (University of Bonn, Germany) provided frozen snakes and valuable comments on snake biology. S.G. was supported in this work by the Federal Ministry of Education, Science and Technology, Germany (BMBF project Biona 01RB0812A). Animal care for the live *G. colubrinus* was provided by M.-C. Klein. The experiments comply with the "Principles of animal care", publication no. 86–23, revised 1985 of the National Institute of Health and also with the current laws of Germany. Figure 1a was reproduced/adapted with permission from *The Journal of Experimental Biology*, Barbakadze N, Enders S, Gorb S, Arzt E (2006) Local mechanical properties of the head articulation cuticle in the beetle *Pachnoda marginata* (Coleoptera, Scarabaeidae). J Exp Biol 209:722–730. doi:10.1242/jeb.0206.

References

Alexander NJ (1970) Comparison of α and β keratin in reptiles. Z Zellforsch 110:153–165

Alibardi L, Sawyer RH (2002) Immunocytochemical analysis of beta keratins in the epidermis of chelonians, lepidosaurians, and archosaurians. J Exp Zool 293:27–38

Alibardi L, Toni M (2006a) Cytochemical, biochemical and molecular aspects of the process of keratinization in the epidermis of reptilian scales. Prog Histochem Cytochem 40:73–134

Alibardi L, Toni M (2006b) Immunological characterization and fine localization of lizard beta-keratin. J Exp Zool 306B:528–538

Alibardi L, Toni M (2006c) Immunolocalization and characterization of beta-keratins in growing epidermis of chelonians. Tissue Cell 38:53–63

Arzt E, Enders S, Gorb S (2002) Towards a micromechanical understanding of biological surface devices. Z Metallkunde 93:345–351

Astbury WT, Bell FO (1939) X-ray data on the structure of natural fibres and other bodies of high molecular weight. Tabulae Biol 17:90–112

Baden HP, Maderson PFA (1970) Morphological and biophysical identification of fibrous proteins in the amniote epidermis. J Exp Zool 174:225–232

Banerjee TK, Mittal AK (1978) Histochemistry of the epidermis of the checkered water snake *Natrix piscator* (Colubridae, Squamata). J Zool 185:415–435

Barbakadze N, Enders S, Gorb S, Arzt E (2006) Local mechanical properties of the head articulation cuticle in the beetle *Pachnoda marginata* (Coleoptera, Scarabaeidae). J Exp Biol 209:722–730

Baumgartner W, Saxe F, Weth A, Hajas D, Sigumonrong D, Emmerlich J, Singheiser M, Böhme W, Schneider JM (2007) The sandfish's skin: morphology, chemistry and reconstruction. J Bionic Eng 4:1–9

Bonser RHC (2001) The elastic properties of wing and contour feather keratin from the Ostrich *Struthio camelus*. Ibis 143:144–145

Bonser RHC, Purslow PP (1995) The Young's modulus of feather keratin. J Exp Biol 198:1029–1033

Carver WE, Sawyer RH (1987) Development and keratinization of the epidermis in the common lizard, *Anolis carolinensis*. J Exp Zool 243:435–443

Dalla Valle L, Toffolo V, Belvedere P, Alibardi L (2005) Isolation of mRNA encoding a glycine-proline-rich β-keratin expressed in the regenerating epidermis of lizard. Dev Dynam 234:934–947

Deuschle J (2008) Mechanics of soft polymer indentation. Dissertation, Max Planck Institute for Metals Research Stuttgart and Institute for Metallography of the University of Stuttgart

Deuschle J, Enders S, Arzt E (2007) Surface detection in nanoindentation of soft polymers. J Mater Res 22:3107–3119

Ebenstein DM, Pruitt LA (2006) Nanoindentation of biological materials. Nano Today 1:26–33

Enders S, Barbakadze N, Gorb SN, Arzt E (2004) Exploring biological surfaces by nanoindentation. J Mater Res 19:880–887

Farren L, Shayler S, Ennos AR (2004) The fracture properties and mechanical design of human fingernails. J Exp Biol 207:735–741

Filshie BK, Rogers GE (1962) An electron microscope study of the fine structure of feather keratin. J Biophys Biochem Cytol 13:1–12

Fong H, Sarikaya M, White SN, Snead ML (2000) Nano-mechanical properties profiles across dentin–enamel junction of human incisor teeth. Mat Sci Eng 7:119–128

Fraser RDB, MacRae TP (1980) Molecular structure and mechanical properties of keratin. In: Vincent JFV, Currey JD (eds) The mechanical properties of biological materials. Symposia of the Society for Experimental Biology

Furch E, Marchuk D (1983) Type I and type II keratins have evolved from lower eukaryotes to from the epidermal intermediate filaments in mammalian skin. Proc Natl Acad Sci USA 80:5857–5861

Fusayama T, Maeda T (1968) Effect of pulpectomy on dentin hardness. J Dent Res 48:452–460

Gibson LJ, Ashby MF (1988) Cellular solids: structures and properties. Pergamon Press, New York

Goslar HG (1958) Beiträge zum Häutungsvorgang der Schlangen. Acta Histochem 5:182–212

Gregg K, Rogers GE (1986) Feather keratins: composition, structure and biogenesis. In: Bereither-Hahn J, Matoltsy GA, Sylvia-Richards K (eds) Biology of the integument: vertebrates, vol 2. Springer, New York, pp 666–694

Huber G, Orso S, Spolenak R, Wegst UGK, Enders S, Gorb SN, Arzt E (2008) Mechanical properties of a single gecko seta. Int J Mater Res 2008:1113–1118

Irish FJ, Williams EE, Seling E (1988) Scanning electron microscopy of changes in the epidermal structure occurring during the shedding cycle in squamate reptiles. J Morphol 197:105–126

Landmann L (1979) Keratin formation and barrier mechanisms in the epidermis of *Natrix natrix* (Reptilia: Serpentes): an ultrastructural study. J Morphol 162:93–126

Landmann L (1986) Biology of the integument. In: Bereither-Hahn J, Matoltsy GA, Sylvia-Richards K (eds) The skin of reptiles, Chap 9: Epidermis and dermis. Springer, Heidelberg, pp 150–185

Lettington AH (1998) Applications of diamond-like carbon thin films. Carbon 36:555–560

Licht P, Bennett AF (1972) A scaleless snake: tests of the role of reptilian scales in water loss and heat transfer. Copeia 4:702–707

Maderson PFA (1964) The skin of lizards and snakes. B J Herpet 3:151–154

Maderson PFA, Rabinowitz B, Tandler B, Alibardi L (1998) Ultrastructural contributions to an understanding of the cellular mechanisms involved in lizard skin shedding with comments on the function and evolution of a unique lepidosaurian phenomenon. J Morphol 236:1–24

Matoltsy AG (1976) Keratinization. J Invest Dermatol 67:20–25

Mattison C (1995) The encyclopedia of snakes. Cassel & Co, London

Mercer EH (1961) Keratin and keratinization. Pergamon Press, Inc, Oxford

Moran P, Towler MR, Chowdhury S, Saunders J, German MJ, Lawson NS, Pollock HM, Pillay L, Lyons D (2007) Preliminary work on the development of a novel detection method for osteoporosis. J Mater Sci 18:969–974

O'Guin WM, Galvin S, Schermer A, Sun TT (1987) Patterns of keratin expression define distinct pathways of epithelial development and differentiation. Curr Top Dev Biol 22: 97–125

Oliver WC, Pharr GM (1992) An improved technique for determining hardness and elastic modulus using load and displacement sensing indentation experiments. J Mater Res 7:1564–1583

Oliver WC, Pharr GM (2004) Measurement of hardness and elastic modulus by instrumented indentation: advances in understanding and refinements in methodology. J Mater Res 19:3–20

Rechenberg I, El Khyari AR (2004) Der Sandskink der Sahara—Vorbild für Reibungs- und Verschleißminderung. http://www.bionik.tuberlin.de/institute/festo04.pdf,Berlin

Sawyer RH, Glenn T, French JO, Mays B, Shames RB, Barnes GL, Rhodes W, Ishikawa Y (2000) The expression of beta keratins in the epidermal appendages of reptiles and birds. Am Zool 40:530–539

Toni M, Alibardi L (2007) Alpha- and beta-keratin of the snake epidermis. Zoology 110:41–47

Wang RZ, Weiner S (1998) Strain-structure relations in human teeth using Moire fringes. J Biomech 31:135–141

Wei G, Bhushan B, Torgerson PM (2005) Nanomechanical characterization of human hair using nanoindentation and SEM, vol 105. Elsevier, Amsterdam, pp 248–266

Wyld JA, Brush AH (1979) The molecular heterogeneity and diversity of reptilian keratins. J Mol Evol 12:331–347

Xu Z, Rowcliffe D (2002) Nanoindenation on diamond-like carbon and alumina coatings. Surf Coat Technol 161:44–51

Xu HHK, Smith DT, Jahanmir S, Romber E, Kelly JR, Thompson VP, Rekow ED (1998) Indentation damage and mechanical properties of human enamel and dentin. J Dent Res 77:472–480

Zheng J, Zhou ZR, Zhang J, Li H, Yu HY (2003) On the friction and wear behaviour of human tooth enamel and dentin, vol 255. Elsevier, Amsterdam, pp 967–974